Journal of Materials Chemistry A

PAPER

View Article Online
View Journal | View Issue



Cite this: J. Mater. Chem. A, 2015, 3, 7332

# 1,4-Bis(trimethylsilyl)-2,5-dimethoxybenzene: a novel redox shuttle additive for overcharge protection in lithium-ion batteries that doubles as a mechanistic chemical probe†

Jinhua Huang,[ab] Ilya A. Shkrob,[b] Peiqi Wang,[b] Lei Cheng,[ac] Baofei Pan,[ab] Meinan He,[b] Chen Liao,[ab] Zhengcheng Zhang,[b] Larry A. Curtiss[ac] and Lu Zhang*[ab]

Received 3rd February 2015
Accepted 25th February 2015

DOI: 10.1039/c5ta00899a

www.rsc.org/MaterialsA

A novel redox shuttle additive, 1,4-bis(trimethylsilyl)-2,5-dimethoxybenzene (BTMSDB), is shown to deliver superb overcharge protection of $LiFePO_4$ electrode in Li-ion batteries. Using this molecule as a chemical probe, we trace the cause of the eventual failure of this additive to the gradual loss of steric protection in the corresponding radical cation, providing the much needed mechanistic insight in the factors controlling the long-term efficiency of overcharge protection.

## Introduction

Rechargeable lithium-ion batteries (LIBs) are widely used in portable electronics and transportation vehicles due to their high specific capacity and energy density, long shelf life and lack of memory effect.[1,2] Currently, safety issues associated with LIBs are limiting their use in many areas, such as electric grid and electric vehicle applications.[3] Among these issues, overcharge abuse is a serious concern in serially connected batteries that have different capacities. In this configuration, low-capacity cells become fully charged before high-capacity cells reach the end-of-charge condition. As the electric current becomes forced through the low-capacity cells, the potential can increase beyond the acceptable limit thereby causing electrolyte breakdown, over-delithiation of the cathode, gas evolution, thermal runaway, and even explosion.[4]

To prevent this overcharge, commercially available LIBs are typically protected by the external electronic devices that add complexity, volume and cost to the system.[4] A less costly approach would be incorporating the so-called redox shuttle additives directly into the electrolyte to provide the intrinsic chemical protection.[4] These additives are electrochemically reversible molecules that are inactive during normal battery charging, but become oxidized when the potential increases above the end-of-charge potential of the cathode material. These compounds shunt the extra current through "oxidation–diffusion–reduction–back diffusion" cycles, *i.e.* their molecules are oxidized at the surface of the cathode, and the electrochemically generated radical cations diffuse to the anode where they become reduced before diffusing back to the cathode as neutral molecules, "shuttling" between the electrodes. This cycle repeats itself until the redox shuttle molecules are consumed in the irreversible side reactions.

Over the past decade, much effort has been invested into the development of redox shuttle molecules suitable for overcharge protection of LIBs. The ferrocene,[5] 2,2,6,6-tetramethylpiperinyl-oxide (TEMPO)[6] and phenothiazine[7,8] based platforms have been examined. Although some of these compounds exhibit remarkable chemical and electrochemical stability, their redox potentials are insufficient for the commercially used $LiFePO_4$ cathode that operates at 3.5 V *vs.* $Li/Li^+$. Generally, the redox potential of a redox shuttle molecule should be at least 0.3 V higher than the end-of-charge potential of the cathode in order to minimize the interference with the normal battery charging so that the self-discharge can be circumvented.[9] For this reason, the alkoxybenzene derivatives began to attract the increased attention due to their higher redox potentials and tunable physical and electrochemical properties.[9–12] By surveying sundry compounds of this class, Dahn *et al.* empirically found that 2,5-di-*tert*-butyl-1,4-dimethoxybenzene (DDB, Fig. 1) exhibited particularly robust overcharge protection.[11] DDB is electrochemically reversible at 3.9 V *vs.* $Li/Li^+$ and it can provide 300 + cycles for overcharge protection of $LiFePO_4$ cathode with 100% overcharge per cycle. Several rationales have been given to account for this remarkable electrochemical stability.[13,14] Specifically, the incorporation of two bulky *tert*-butyl groups at 2,5-positions in the benzene ring of 1,4-dimethoxybenzene (DMB) is thought to protect the electrochemically generated radical cation against undesirable side reactions such as

[a]Joint Center for Energy Storage Research, Argonne National Laboratory, IL 60439, USA. E-mail: luzhang@anl.gov

[b]Chemical Sciences and Engineering Division, Argonne National Laboratory, IL 60439, USA

[c]Materials Science Division, Argonne National Laboratory, IL 60439, USA

† Electronic supplementary information (ESI) available. See DOI: 10.1039/c5ta00899a

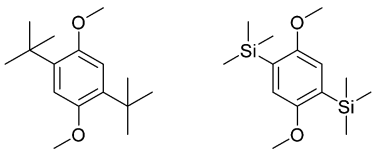


Fig. 1 The chemical structures of DDB and BTMSDB.

disproportionation, radical addition, and cross-recombination. Despite these many advantages, DDB also has several shortcomings, including the low solubility and relatively low redox potential. The subsequent studies sought to improve these properties,[13–18] but most of these studies focused on the modification of the *methoxy* moiety while retaining the protective di-*tert*-butyl groups. Herein, we break with this pattern and report a novel redox shuttle additive, 1,4-bis(trimethylsilyl)-2,5-dimethoxybenzene (BTMSDB, Fig. 1), through the modification of the protective groups in DDB. Below we demonstrate that BTMSDB provides superb overcharge protection of $LiFePO_4$/MCMB (mesocarbon microbead) cell without adversely affecting the discharge capacity of the cell.

While all of the redox shuttle additives eventually fail as protective agents, the mechanistic causes for this failure are insufficiently understood. The main motivation for our study was to address this problem through incorporation of a chemical marker, *viz.* the silicon heteroatom, in order to provide a convenient way of tracking the decomposition products by means of elemental analysis of the cell components. This option does not exist for organic molecules like DDB, in which case the isotope labelling is required. The difficulty of this chemical approach is in transforming a molecule into a probe without compromising its performance as the redox shuttle, and BTMSDB is unique in this respect. Using this advantage, by means of the direct comparison of DDB and BTMSDB and the support from our spectroscopic and computational analyses, we were able to conclusively demonstrate that the eventual failure of BTMSDB (and, possibly, other redox shuttles of this class) is due to the gradual loss of the protective groups in the corresponding radical cation. This ability to link the specific cause and the long-term effect makes our study the first of its kind.

## Experimental section

### Materials

1,4-dimethoxybenzene (99%), 2,5-di-*tert*-butylhydroquinone (99%), tetramethylethylenediamine (99%), *n*BuLi (2.5 M in hexanes), chlorotrimethylsilane (≥99%), sodium hydride (60% dispersion in mineral oil), iodomethane (99.5%), butyronitrile (≥99%), bis(trifluoromethane) sulfonimide lithium salt (LiTFSI, 99.95%), [bis(trifluoroacetoxy)iodo]benzene (97%), ethylene carbonate (99%, anhydrous), diethyl carbonate (≥99%, anhydrous), propylene carbonate (99.7%, anhydrous) and lithium ribbon (99.9%, 0.75 mm thick) were purchased from Sigma-Aldrich. Lithium bis(oxalato)borate (LiBOB) was purified by the Materials Engineering Research Facility at Argonne National Laboratory. LiTFSI was dried in the vacuum oven at 70 °C for 12 hours before use; all other chemicals were used as supplied.

### BTMSDB synthesis

To a mixture of 1,4-dimethoxybenzene (6.91 g, 50 mmol) and tetramethylethylenediamine (18.71 mL, 125 mL) in anhydrous $Et_2O$ (200 mL) was added *n*BuLi (44 mL, 2.5 M in hexanes, 110 mmol) dropwise at room temperature under nitrogen. After stirring for 12 hours, chlorotrimethylsilane was slowly added to this reaction mixture at 0 °C. The mixture was stirred for the additional 4 h and subsequently quenched with water. The organic layer was separated, and the aqueous layer was extracted with ethyl acetate. The combined organic layers were washed with water and brine and dried over $Na_2SO_4$. After concentration *in vacuo*, the residue was purified by flash column chromatography (silica gel, eluted with ethyl acetate/hexanes = 1/40) to yield BTMSDB (10.72 g, 76%) as a white solid. $^1$H NMR (500 MHz, $CDCl_3$) $\delta$ 6.87 (s, 2H), 3.79 (s, 6H), 0.27 (s, 18H); $^{13}$C NMR (125 MHz, $CDCl_3$) $\delta$ 158.4, 130.3, 116.3, 55.9, −1.0. See Fig. S1 and S2 in the ESI.†

### DDB synthesis

To a solution of 2,5-di-*tert*-butylhydroquinone (4.45 g, 20 mmol) in anhydrous DMF (50 mL) was added NaH (1.76 g, 60% dispersion in oil, 44 mmol) in small portions under nitrogen. After the gas evolution had ceased, the resulting mixture was stirred at room temperature for 15 min. The iodomethane (4.98 mL, 80 mmol) was added dropwise to this mixture, which was stirred at 40 °C for the additional 2 h. Brine was added slowly to quench the reaction and the resulting mixture was extracted with ethyl acetate. The combined organic layers were washed with water and dried over $Na_2SO_4$. After concentration *in vacuo*, the residue was purified by flash column chromatography (silica gel, eluted with ethyl acetate/hexanes = 1/40) to yield DDB (4.70 g, 94%) as a white solid. $^1$H NMR (500 MHz, $CDCl_3$) $\delta$ 6.88 (s, 2H), 3.86 (s, 6H), 1.42 (s, 18H); $^{13}$C NMR (125 MHz, $CDCl_3$) $\delta$ 151.9, 136.3, 111.6, 55.9, 34.6, 29.8. See Fig. S3 and S4 in the ESI.†

### Electrochemical measurements

All electrochemical experiments were carried out in an argon-filled glove box with the water and oxygen levels <1 ppm. The data were collected using a CHI660D potentiostat (CH Instruments). Cyclic voltammograms (CV) were obtained using a custom-made three-electrode cell with a 2 mm diameter platinum working electrode, a Li-metal counter reference electrode, and a Li-metal counter electrode. 10 mM BTMSDB dissolved in 0.5 M LiBOB in ethyl carbonate and diethyl carbonate (1 : 4, v/v) was used as the electrolyte. The diffusion coefficient was calculated using the Randles–Sevcik equation.

$$I_{ap} = (268, 600)n^{3/2}AD^{1/2}Cv^{1/2} \quad (1)$$

Where $I_{ap}$ is the anodic peak current ($A$), $n$ is the number of the electrons involved in a redox reaction, $A$ is the electrode area

($cm^2$), $D$ is the diffusion coefficient ($cm^2\ s^{-1}$), $C$ is the concentration of the redox shuttle (mol $cm^{-3}$), and $\nu$ is the scan rate ($V\ s^{-1}$).

The overcharge test was conducted in $LiFePO_4$/Li or $LiFePO_4$/MCMB 2032 coin cells with celgard 2325 as a separator. The $LiFePO_4$ electrode is composed of 82% $LiFePO_4$ active material, 8% super P carbon black and 10% PVDF binder. The MCMB electrode is composed of 90% MCMB active material, 2% super P carbon black and 8% PVDF binder. These cells were charged using a constant current to 200% capacity (100% overcharge ratio) or until a specific upper cutoff voltage was reached (normally 4.95V *vs.* $Li/Li^+$), whichever occurred first. After the charging process, the cells were discharged to a normal cutoff voltage using the same constant current.

### Chemical oxidation

The [bis(trifluoroacetoxy)iodo]benzene (25 mmol) was added to a solution of BTMSDB or DDB (5 mmol) in butyronitrile (5 mL) containing trifluroacetic acid (25 mmol).

### Electrochemical oxidation

The constant potential bulk electrolysis was performed in a three-electrode bulk electrolysis cell (BASi) with a high surface reticulated vitreous carbon serving as a working electrode, Li metal strip enclosed in Vycor-fritted or ceramic fritted glass tube as a reference electrode and a counter electrode, respectively. The electrolyte was 1 mM BTMSDB or DDB in 0.5 M LiTFSI in 30 mL PC (<10 ppm of water) continuously stirred at 700 rpm during the electrolysis. The potential was fixed at 4.10 V and the state of charge was 90%.

### Electron paramagnetic resonance (EPR) measurements

Electrochemically and/or chemically oxidized liquid solutions were placed in graduated glass capillaries and sealed inside of borosilicate glass tubes that were subsequently transferred to the resonator of a Bruker ESP300E X band EPR spectrometer. The magnetic field and hyperfine coupling constants are given in the units of Gauss ($1\ G = 10^{-4}\ T$). The first-derivative EPR spectra were obtained with the modulation frequency of 100 kHz and the modulation amplitude of 0.1 or 0.2 G. No saturation effects were observed as the microwave power varied between 0.002 and 2 mW; the EPR spectra shown in the text were obtained at 2 mW. WINSIM suite Version 0.98 (NIH) was used to analyze these EPR spectra.

### Optical absorption measurements

For absorption measurements, the same electrochemically oxidized solutions were placed in a 1 mm optical path quartz cuvette and spectra were obtained using an Olis Cary 14 spectrometer. The decay kinetics were collected at 466 nm, where only the radical cations absorb analyzing light.

### Density functional theory (DFT) calculations

The calculations of the hfcc's and radical structures were carried out using a DFT method with the B3LYP functional and 6–31 + G(d, p) basis set from Gaussian 03. The reaction energies were calculated using the same level of theory with entropic corrections from the frequency calculations and solvation energy corrections calculated with the PCM SCRF solvation model.

### Scanning electron microscopy (SEM) and energy dispersive X-ray spectroscopy (EDX)

The SEM and EDX examinations were conducted on a high resolution Hitachi S-4700 scanning electron microscope with a field emission electron source to characterize morphology and analyze elements of the harvest electrodes.

## Results and discussion

The electrochemical properties of BTMSDB were evaluated using cyclic voltammetry in a Pt/Li/Li three-electrode cell containing 10 mM BTMSDB in ethyl carbonate and diethyl carbonate (1 : 4 v/v) with 0.5 M lithium bis(oxalato)borate (LiBOB) as the supporting electrolyte. LiBOB is a well-known battery additive for the protection of the electrode surface[19–21] and it was previously used for overcharge tests by Dahn *et al.*[12] An automatic iR correction with a compensation level of 90% was applied before each CV measurement to eliminate the iR drop due to the solution resistance. As shown in Fig. 2a, BTMSDB exhibits well-defined, reversible redox waves with a redox potential at 4.1 V *vs.* $Li/Li^+$, which is determined by the mean of the anodic and cathodic peak values. It is also observed that these redox peaks shift only slightly as a function of the scan rate, as the latter increases from 5 mV $s^{-1}$ to 100 mV $s^{-1}$ under iR compensation. The ratio of anodic and cathodic currents nearly equals unity for all of the scan rates, which suggests good reversibility of the redox reaction (see Table S1 in the ESI†). These results suggest that the trimethylsilyl substitution in the benzene ring provided the sufficient steric protection for the radical cation on the time scale of the CV scans.

Since BTMSDB was found to be electrochemically reversible, its ability to serve as a redox shuttle for overcharge protection was further examined. The diffusion coefficient is an important parameter controlling the efficiency of the redox shuttle molecule to shunt the extra current during the overcharge. This

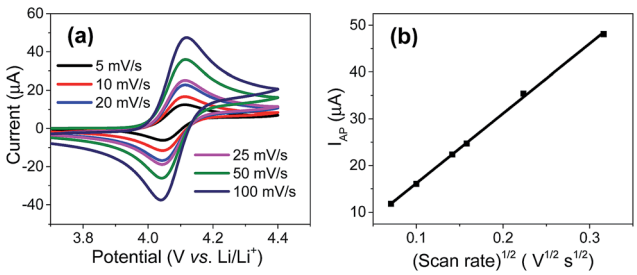


Fig. 2 a) Cyclic voltammograms of 10 mM BTMSDB in 0.5 M LiBOB in ethyl carbonate and diethyl carbonate (1 : 4 v/v) using Pt/Li/Li three-electrode at various scan rates; (b) plots of $I_{ap}$ *vs.* (scan rate)$^{1/2}$ for BTMSDB.

 

diffusion coefficient was estimated plotting the anodic peak current ($I_{ap}$) *vs.* the square root of the scan rate (Fig. 2b). The linearity of this plot suggests the occurrence of a diffusion-controlled reaction. Using eqn (1), an estimate of 3.09 x $10^{-6}$ $cm^2$ $s^{-1}$ was obtained for the diffusion coefficient $D$ of the radical cation, which is 2X greater than the value reported for DDB.[12] This more rapid diffusion can result in the accelerated current shutting and faster recovery of the redox shuttle.

The CV profile in Fig. 2a implies that BTMSDB is suitable for overcharge protection of $LiFePO_4$ cathode, whose end-of-charge potential (3.5 V *vs.* $Li/Li^+$) is 0.6 V lower than that of BTMSDB. Fig. 3a shows the plots of voltage *vs.* capacity for $LiFePO_4$/Li and $LiFePO_4$/MCMB 2032 coin cells containing 0.1 M BTMSDB in 0.5 M LiBOB in ethyl carbonate and diethyl carbonate (1 : 4 v/v). These coin cells were first charged at C/10 rate for 20 h with 100% overcharge and then fully discharged at the same C/10 rate. As shown in Fig. 3a, the charge curve exhibits two distinctive plateaus for each cycle. The first one appearing at ~3.4/3.5 V (*vs.* MCMB/Li) during the first 10 h represents the normal charging process to attain the full lithium ion capacity of $LiFePO_4$ cathode. Following this initial stage, the voltage increases to ~4.0/4.1 V (*vs.* MCMB/Li), where the second plateau is observed over the next 10 h. The potential at which the second plateau is attained corresponds exactly to the redox potential of BTSMDB (*cf.* Fig. 2a), implicating its oxidation. The overcharge cycling continued until the redox shuttle molecules were consumed. As indicated by the capacity retention profiles shown in Fig. 3b and c, the long-term overcharge performance strongly depends upon the anode composition. Under the test conditions stipulated above, the $LiFePO_4$/MCMB cell lasted over 35 cycles before the charge capacity started to drop due to the depletion of the redox shuttle. In contrast, the $LiFePO_4$/Li cell operated for just 18 cycles. This difference in the performance can be attributed to undesired side reactions of the radical cation of BTMSDB upon the contact with a more reductive anode (see below). This overcharge tolerance for the anodes follows the trend previously reported by Dahn *et al.* and Amine *et al.* for other systems.[15,16]

The overcharge performance of redox shuttle improved when the concentration of BTMSDB was increased; such dependence was observed in other DMB based systems, too.[14] For instance, when the concentration of the shuttle was increased to 0.15 M, robust cell operation extended over 81 cycles (Fig. 3d) indicating superb electrochemical stability. Furthermore, the addition of BTMSDB negligibly affected the cycling performance under the overcharge conditions. As shown in Fig. 3d, the discharge capacity retention exceeded 94% over the entire overcharge process. While many of the redox shuttles have been used for overcharge protection of $LiFePO_4$ and 4 V mixed oxide electrode materials, most of these compounds suffered from severe capacity loss, which in some cases exceeded 50%.[14,15,22–25] The competing demands of overcharge protection and maintaining discharge capacity present a formidable challenge for redox shuttle development. To our knowledge, BTMSDB is a rare example of a compound that is capable of providing the overcharge protection of $LiFePO_4$ electrode *without* the concomitant capacity loss.

The overcharge performance of BTMSDB was inferior to DDB in a $LiFePO_4$/graphite coin cell (81 *vs.* > 300 cycles). In order to compare the performance of these two redox shuttles under the same conditions, two $LiFePO_4$/Li coin cells containing 0.1 M redox shuttle in 0.5 M LiBOB in ethyl carbonate and diethyl carbonate (1 : 4 v/v) were assembled and charged at C/10 until the upper cutoff of 5 V was reached.[26] As shown in Fig. 4, two plateaus at 3.5 and 4.1 V *vs.* $Li/Li^+$ were observed for BTMSDB and DDB, respectively. The second plateau indicates that BTMSDB and DDB have the same redox potential at 4.1 V *vs.* $Li/Li^+$. Similarly to Fig. 3a, the first plateau at 3.5 V represents the normal charging process. Subsequently, the voltage rapidly increased to 4.1 V and stayed constant until it reached the upper

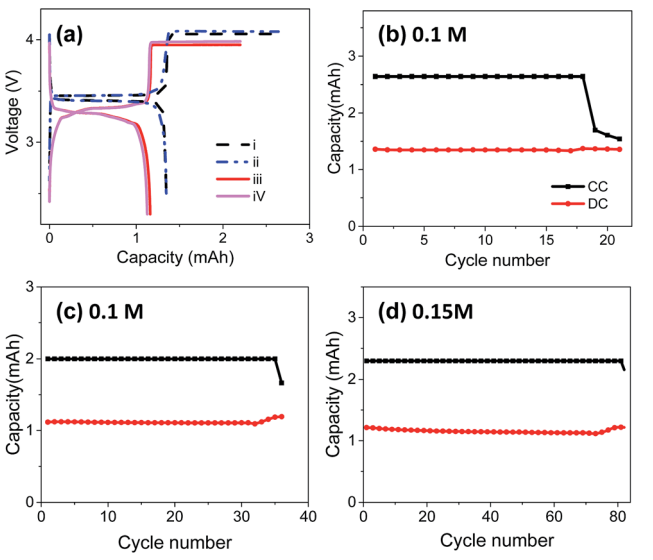


Fig. 3 (a) Voltage *vs.* capacity profiles of the $LiFePO_4$/Li and $LiFePO_4$/MCMB coin cells containing 0.1 M BTMSDB in 0.5 M LiBOB in ethyl carbonate and diethyl carbonate (1 : 4 v/v), the charging rate is C/10 and the overcharge ratio is 100%. Trace i was the 3rd cycle of $LiFePO_4$/Li; trace ii was the 10th cycle of $LiFePO_4$/Li, trace iii was the 5th cycle of $LiFePO_4$/MCMB, trace iV was the 20th cycle of $LiFePO_4$/MCMB. Capacity retention profiles for (b) 0.1 M BTMSDB, $LiFePO_4$/Li, (c) 0.1 M BTMSDB, $LiFePO_4$/MCMB, and (d) 0.15 M BTMSDB, $LiFePO_4$/MCMB. In panel b, CC and DC stand for the charge capacity and discharge capacity, respectively.

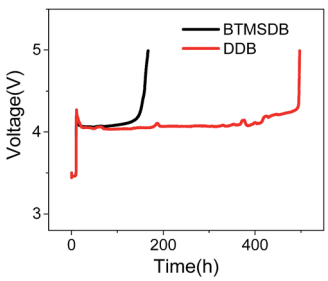


Fig. 4 The constant charging profiles of the $LiFePO_4$/Li coin cells containing 0.1 M redox shuttle in 0.5 M LiBOB in ethyl carbonate and diethyl carbonate (1 : 4 v/v) at C/10 until 5 V was reached.

cutoff of 5 V. The BTMSDB cell failed after 168 h whereas the DDB cell failed after 498 h.

The observed difference in the overcharge performance of BTMSDB *vs.* DDB can be attributed to the relatively poor stability of the C–Si bond in the corresponding radical cation. In order to verify this hypothesis, the electrolyte and the electrodes of coin cells containing 0.15 M BTMSDB were harvested after the test. The liquid electrolyte was analyzed using $^{1}$H NMR (nuclear magnetic resonance) spectroscopy and GCMS (gas chromatography-mass spectrometry). Both of these methods indicated the presence of DMB in the solution (see Fig. S5–S7 in the ESI†). The elimination of the trimethylsilyl groups was also suggested by the EDX spectra of the harvested electrodes shown in Fig. 5. Apart from C, O, P and Fe that are intrinsic to the cathode material, Si was observed. This silicon can be resulting only from the decomposition of BTMSDB. After the cleavage of the trimethylsilyl group(s), the decomposition product(s) (which is likely to be DMB) was unable to function as a redox shuttle. Therefore, it is not surprising to find that the overcharge performance of BTMSDB was less robust comparing to DDB. The insets in Fig. 5 present the scanning electron microscopy (SEM) images of the harvested $LiFePO_4$ cathode and MCMB anode. It is seen that the particle structure of both electrodes was maintained after the cycling. Thus, the deposition of the decomposition product(s) of BTMSDB had no visible effect on the electrode surface, which is consistent with the capacity retention profiles shown in Fig. 3d.

To further elucidate the difference between BTMSDB and DDB, density functional theory (DFT) calculations for gas-phase species were carried out. These calculations indicate that the elimination of the trimethylsilyl radical from $BTMSDB^{+\bullet}$ would be prohibitively endergonic (by *ca.* 4 eV *vs.* 3.6 eV for *tert*-butyl radical from $DDB^{+\bullet}$), suggesting that the reaction involves the formation of a radical residue of the parent molecule (see Fig. S8 in the ESI†). Had the reaction involved the formation of the corresponding trimethylsilyl carbocation, it would still be endergonic, so binding of the eliminated carbocation to a solvent molecule is required. Another potential way to facilitate this reaction is the internal H atom transfer between the methoxy group and the aromatic ring, which stabilizes the resulting radical. With this radical stabilization and the solvent serving as the acceptor of the eliminated carbocation, the loss of the trimethylsilyl group from $BTMSDB^{+\bullet}$ becomes endergonic by 0.65 eV, whereas the same reaction for $DDB^{+\bullet}$ is endergonic by 1.76 eV. The difference in the enthalpies mainly stems from the energetics of the Si–O bond in the formation of the solvent adduct (see Fig. S8 in the ESI†). This reaction can be facilitated further by the presence of a base, such as an alkyl-carbonate anion generated through the decomposition of the carbonate solvent on the surface of the anode during the solid-electrolyte interphase (SEI) formation.[27–29] We suggest that the slow reactions with the carbonate solvent and more rapid surface reactions involving these carbonate bases in the SEI cause gradual loss of the protective trimethylsilyl groups and eventually limit the lifetime of $BTMSDB^{+\bullet}$ radical cations in the electrochemical cell.

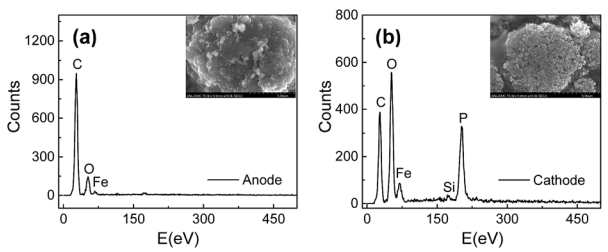


Fig. 5 The EDX spectra and SEM images of (a) anode and (b) cathode harvested from the $LiFePO_4$/MCMB coin cells containing 0.15 M BTMSDB in 0.5 M LiBOB in ethyl carbonate and diethyl carbonate (1 : 4 v/v).

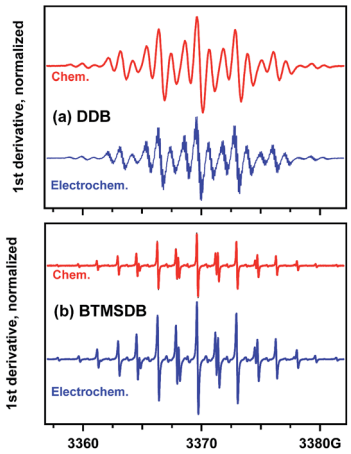


Fig. 6 The normalized first-derivative EPR spectra of chemically and electrochemically oxidized (a) DDB and (b) BTMSDB solutions.

To identify these postulated reaction intermediates, the radical cations of BTMSDB and DDB were generated in solution. The first-derivative electron paramagnetic resonance (EPR) spectra obtained are shown in Fig. 6, and the hyperfine coupling constants for the observed radical cations are given in Table S2 in the ESI.† For comparison, the hyperfine constants calculated using the DFT method for the gas-phase species are given in the same table. Our results indicate that the EPR signals observed in the chemically and electrochemically oxidized solutions originate exclusively from the corresponding radical cations. No π-stack sandwich dimer[30,31] or multimer[32] radical cations that frequently occur for benzene derivatives were observed. Concomitant with the development of EPR signals, the strong absorption bands of the corresponding radical cations were observed at 310, 440, and 464 nm for DDB and 308, 442, and 466 nm for BTMSDB (Fig. S9 in the ESI†). The examination of the decay kinetics given in the same plot indicate that $DDB^{+\bullet}$ is significantly more stable than $BTMSDB^{+\bullet}$ even in the solvent bulk, thereby validating the suggested side reaction suggested in Fig. S8 in the ESI.†

## Conclusion

Currently, little is known about the mechanisms for the eventual failure of the redox shuttles in LIBs. The unique advantage

 

of BTMSDB (Fig. 1) as a redox shuttle is the combination of the superb performance and the ease of tracing the products of its decomposition through analysis. BTMSDB exhibits reversible redox potential at 4.1 V *vs.* $Li/Li^+$, which is suitable for overcharge protection of $LiFePO_4$ cathode. We demonstrate that BTMSDB provides overcharge protection to the $LiFePO_4$/MCMB coin cells for 81 cycles, without the contaminant discharge capacity loss. By the current standards, this is a remarkable performance. Still, the direct comparison of BTMSDB and DDB under the same conditions indicates that DDB provides 3X longer overcharge protection than BTMSDB despite the striking structural similarity. This difference stems from a side reaction of BTMSDB radical cation that eliminates the protective trimethylsilyl groups. Both the radical cation and the products of decomposition were directly observed. This reaction can become more facile on the surface of the anode, where it is facilitated by alkylcarbonate bases generated *via* the electrolyte breakdown during SEI formation. Our study suggests that the improvement strategy for the redox shuttles should be advanced in the full awareness of such detrimental side reactions, as their occurrence undermines the long term performance of the protected LIBs. Our study also provides a still rare example of a system where the eventual failure of the robust redox shuttle has been traced to a specific chemical cause. The generality of this mechanistic insight needs to be further explored.

## Acknowledgements

This work was supported by the U. S. Department of Energy, Office of Science, Office of Basic Energy Sciences, Division of Chemical Sciences, Geosciences and Biosciences under contract No. DE-AC02-06CH11357; it was also supported as part of the Joint Center for Energy Storage Research (JCESR), an Energy Innovation Hub funded by the U.S. Department of Energy, Office of Science, Basic Energy Sciences.

## Notes and references

1 J. M. Tarascon and M. Armand, *Nature*, 2001, **414**, 359–367.
2 B. Dunn, H. Kamath and J.-M. Tarascon, *Science*, 2011, **334**, 928–935.
3 M. Jacoby, *Chem. Eng. News*, 2007, **85**(51), 26–28.
4 Z. Chen, Y. Qin and K. Amine, *Electrochim. Acta*, 2009, **54**, 5605–5613.
5 M. N. Golovin, D. P. Wilkinson, J. T. Dudley, D. Holonko and S. Woo, *J. Electrochem. Soc.*, 1992, **139**, 5–10.
6 L. M. Moshurchak, C. Buhrmester, R. L. Wang and J. R. Dahn, *Electrochim. Acta*, 2007, **52**, 3779–3784.
7 C. Buhrmester, L. Moshurchak, R. L. Wang and J. R. Dahn, *J. Electrochem. Soc.*, 2006, **153**, A288–A294.
8 S. Ergun, C. F. Elliott, A. P. Kaur, S. R. Parkin and S. A. Odom, *Chem. Commun.*, 2014, **50**, 5339–5341.
9 J. Chen, C. Buhrmester and J. R. Dahn, *Electrochem. Solid-State Lett.*, 2005, **8**, A59–A62.
10 M. Adachi, K. Tanaka and K. Sekai, *J. Electrochem. Soc.*, 1999, **146**, 1256–1261.
11 C. Buhrmester, J. Chen, L. Moshurchak, J. Jiang, R. L. Wang and J. R. Dahn, *J. Electrochem. Soc.*, 2005, **152**, A2390–A2399.
12 L. M. Moshurchak, C. Buhrmester and J. R. Dahn, *J. Electrochem. Soc.*, 2005, **152**, A1279–A1282.
13 Z. Zhang, L. Zhang, J. A. Schlueter, P. C. Redfern, L. Curtiss and K. Amine, *J. Power Sources*, 2010, **195**, 4957–4962.
14 L. Zhang, Z. Zhang, P. C. Redfern, L. A. Curtiss and K. Amine, *Energy Environ. Sci.*, 2012, **5**, 8204–8207.
15 L. M. Moshurchak, W. M. Lamanna, M. Bulinski, R. L. Wang, R. R. Garsuch, J. Jiang, D. Magnuson, M. Triemert and J. R. Dahn, *J. Electrochem. Soc.*, 2009, **156**, A309–A312.
16 W. Weng, Y. Tao, Z. Zhang, P. C. Redfern, L. A. Curtiss and K. Amine, *J. Electrochem. Soc.*, 2013, **160**, A1711–A1715.
17 W. Weng, Z. Zhang, P. C. Redfern, L. A. Curtiss and K. Amine, *J. Power Sources*, 2011, **196**, 1530–1536.
18 J. Huang, L. Cheng, R. S. Assary, P. Wang, Z. Xue, A. K. Burrell, L. A. Curtiss and L. Zhang, *Adv. Energy Mater.*, 2014, DOI: 10.1002/aenm.201401782.
19 K. Xu, *Chem. Rev.*, 2004, **104**, 4303–4418.
20 L. Zhang, J. Huang, K. Youssef, P. C. Redfern, L. A. Curtiss, K. Amine and Z. Zhang, *J. Electrochem. Soc.*, 2014, **161**, A2262–A2267.
21 I. A. Shkrob, Y. Zhu, T. W. Marin and D. P. Abraham, *J. Phys. Chem. C*, 2013, **117**, 23750–23756.
22 Z. Chen, Y. Ren, A. N. Jansen, C.-k. Lin, W. Weng and K. Amine, *Nat. Commun.*, 2013, **4**, 1513.
23 Z. Chen and K. Amine, *Electrochem. Commun.*, 2007, **9**, 703–707.
24 M. Taggougui, B. Carré, P. Willmann and D. Lemordant, *J. Power Sources*, 2007, **174**, 1069–1073.
25 K. A. Narayana, M. D. Casselman, C. F. Elliott, S. Ergun, S. R. Parkin, C. Risko and S. A. Odom, *ChemPhysChem*, 2014, DOI: 10.1002/cphc.20142674R1.
26 A. P. Kaur, S. Ergun, C. F. Elliott and S. A. Odom, *J. Mater. Chem. A*, 2014, **2**, 18190–18193.
27 K. Xu, *Chem. Rev.*, 2014, **114**, 11503–11618.
28 I. A. Shkrob, Y. Zhu, T. W. Marin and D. Abraham, *J. Phys. Chem. C*, 2013, **117**, 19255–19269.
29 I. A. Shkrob, Y. Zhu, T. W. Marin and D. Abraham, *J. Phys. Chem. C*, 2013, **117**, 19270–19279.
30 B. Badger and B. Brocklehurst, *Trans. Faraday Soc.*, 1969, **65**, 2582–2587.
31 Y. Itagaki, N. P. Benetis, R. M. Kadam and A. Lund, *Phys. Chem. Chem. Phys.*, 2000, **2**, 2683–2689.
32 K. Okamoto, S. Seki and S. Tagawa, *J. Phys. Chem. A*, 2006, **110**, 8073–8080.